Environmental Science & Technology

Article

Cite This: Environ. Sci. Technol. 2019, 53, 1139−1149

pubs.acs.org/est

Investigating the Heterogeneous Ice Nucleation of Sea Spray Aerosols Using *Prochlorococcus* as a Model Source of Marine Organic Matter

Martin J. Wolf,[†] Allison Coe,[‡] Lilian A. Dove,[†] Maria A. Zawadowicz,[§] Keven Dooley,[‡] Steven J. Biller,[‡] Yue Zhang,[∥,⊥,#] Sallie W. Chisholm,[‡,▽] and Daniel J. Cziczo*[,†,‡]

[†]Department of Earth, Atmospheric, and Planetary Sciences, Massachusetts Institute of Technology, 77 Massachusetts Avenue, Room 54-918, Cambridge, Massachusetts 02139, United States

[‡]Department of Civil and Environmental Engineering, Massachusetts Institute of Technology, 77 Massachusetts Avenue, Room 1-290, Cambridge, Massachusetts 02139, United States

[§]Atmospheric Sciences and Global Change Division, Pacific Northwest National Laboratory, 902 Battelle Boulevard, Richland, Washington 99354, United States

[∥]Department of Environmental Sciences, University of North Carolina at Chapel Hill, 135 Dauer Drive, 166 Rosenau Hall, Chapel Hill, North Carolina 27599, United States

[⊥]Aerodyne Research Incorporated, Center for Aerosol and Cloud Chemistry, 45 Manning Road, Billerica, Massachusetts 01821, United States

[#]Department of Chemistry, Boston College, 2609 Beacon Street, Chestnut Hill, Massachusetts 02467, United States

[▽]Department of Biology, Massachusetts Institute of Technology, 77 Massachusetts Avenue, Room 68-132, Cambridge, Massachusetts 02139, United States

Supporting Information

ABSTRACT: Sea spray is the largest aerosol source on Earth. Bubble bursting mechanisms at the ocean surface create smaller film burst and larger jet drop particles. This study quantified the effects of particle chemistry on the depositional ice nucleation efficiency of laboratory-generated sea spray aerosols under the cirrus-relevant conditions. Cultures of *Prochlorococcus*, the most abundant phytoplankton species in the global ocean, were used as a model source of organic sea spray aerosols. We showed that smaller particles generated from lysed *Prochlorococcus* cultures are organically enriched and nucleate more effectively than larger particles generated from the same cultures. We then quantified the ice nucleation efficiency of single component organic molecules that mimic *Prochlorococcus* proteins, lipids, and saccharides. Amylopectin, agarose, and aspartic acid exhibited similar critical ice saturations, fractional activations, and ice nucleation active site number densities to particles generated from *Prochlorococcus* cultures. These findings indicate that saccharides and proteins with numerous and well-ordered hydrophilic functional groups may determine the ice nucleation abilities of organic sea spray aerosols.

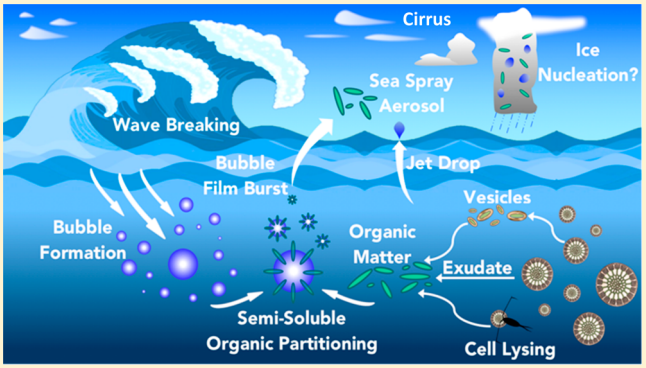

1. INTRODUCTION

The effects of atmospheric aerosols on cloud properties remain the largest source of uncertainty in our understanding of the climate system.[1] Aerosol-induced ice nucleation affects the global radiative budget and hydrological cycle by influencing cloud formation, lifetime, albedo, and precipitation efficiency.[2−5] Aqueous droplets freeze spontaneously via homogeneous nucleation below −38 °C, yet ice can form at lower relative humidities through heterogeneous nucleation on ice nucleating particles (INPs).[6] Deposition nucleation is one mode of heterogeneous nucleation where water vapor deposits directly as solid ice onto the surface of an INP. A thorough understanding of the types, sources, and atmospheric abundances of depositional INPs is lacking, leading to inaccuracies in the representation of cirrus cloud formation in climate models.[7]

Received: September 12, 2018
Revised: December 11, 2018
Accepted: December 27, 2018
Published: December 27, 2018

DOI: 10.1021/acs.est.8b05150
Environ. Sci. Technol. 2019, 53, 1139−1149

Table 1. Particle Compositions and Sizes Tested for Heterogeneous Ice Nucleation Efficiency

category	chemical makeup	particle diameter	g T_g(0/70/90%RH_w)
inorganics			
sodium chloride	NaCl	polydisperse	
synthetic seawater (SSW)	NaCl, $MgCl_2$, KCl, $CaSO_4$, $NaHCO_3$	polydisperse	
Pro99 cell culturing medium	Moore et al. 2017	polydisperse	
proteins and amino acids			
bovine serum albumin		200 nm	
aspartic acid	$C_4H_7NO_4$	200 nm	−11/−52/−93 °C
threonine	$C_4H_9NO_3$	200 nm	−33/−67/−101 °C
arginine	$C_6H_{14}N_4O_2$	200 nm	6/−41/−87 °C
protein mixture	equal mass of above	200 nm	
lipids			
oleic acid	$C_{18}H_{34}O_2$	200 nm	−2/−46/−90 °C
1,2-decanediol	$C_{10}H_{22}O_2$	200 nm	−47/−77/−106 °C
elaidic acid	$C_{18}H_{34}O_2$	200 nm	−2/−46/−90 °C
stearic acid	$C_{18}H_{36}O_2$	200 nm	−1/−45/−89 °C
lipid mixture	equal mass of above	200 nm	
saccharides			
amylopectin	$(C_6H_{10}O_5)_n$	200 nm	NA/63/−25 °C
agarose	$(C_{12}H_{22}O_{11})_n$	200 nm	NA/163/102 °C
raffinose	$C_{18}H_{32}O_{16}$	200 nm	97/37/−63 °C
trehalose	$C_{12}H_{22}O_{11}$	200 nm	64/27/−43 °C
carbohydrate mixture	equal mass of above	200 nm	
***Prochlorococcus* culture**			
whole cell		polydisperse	
lysed cell		polydisperse	
film burst lysed cell		200 nm	
jet drop lysed cell		500 nm	

Inorganic components of sea spray aerosols (SSA) can only activate as depositional INPs below −50 °C.[8−11] The organic components of SSA exhibit several qualities of potentially effective INPs, such as hydrophilic functionality and high porosity from glassy state phase transitions.[12−14] Organic matter is released into bulk seawater by organisms through either normal cellular activity or as a consequence of cell lysis.[15−17] This organic matter can include cell fragments, viruses, vesicles, other biologically derived carbohydrates, lipids, amino acids, and proteins.[18−21] Breaking waves entrain air that scavenges hydrophobic or amphiphilic organic matter as it rises to the surface as bubbles (TOC Figure).[22,23] At the surface microlayer, these bubbles develop a thin organically-enriched film. Submicron fragments of the film are aerosolized up to 20 cm above the ocean surface as the film bursts.[24] Larger and more inorganic jet droplets are ejected as the depression rapidly fills with water.[6,25] Microbial metabolisms regulate the solubility of organic matter in the water column and can also influence the organic mass fraction of SSA.[26]

The importance of SSA as a source of depositional INPs remains uncertain. Heterogeneous ice residuals from cirrus altitudes near marine regions exhibit chemical signatures of SSA.[27] Organic SSA from North Atlantic sea surface microlayer samples depositionally nucleated at relative humidities 10−28% lower than inorganic SSA from subsurface water samples.[23] Various plankton species' exudates are effective INPs in the cirrus regime.[9,28] Despite these findings, the exact nature of the ice nucleation active organic components of SSA remains elusive.

In this study, we explore the relationships between particle chemistry and depositional ice nucleation efficiency. Nucleation efficiency is quantified by the temperatures and supersaturations required to initiate ice nucleation on one in 10^4 of the measured aerosol particles, fractional activation, and ice nucleation active site densities.[29,30] We employ cultures of the marine cyanobacterium *Prochlorococcus* as a representative source of marine organic matter and measure the ice nucleation efficiency of laboratory-generated SSA over a cirrus-relevant temperature and supersaturation range. These cyanobacteria are among the most abundant organisms on Earth, found in surface waters throughout the open ocean between 40°N to 40°S and achieving concentrations up to 2.5 × 10^5 cells mL^{-1}, accounting for up to 50% of the chlorophyll content in some regions.[31,32] We then investigate the depositional ice nucleation ability of single component organic particles composed of amino acids and proteins (aspartic acid, arginine, threonine, and bovine serum albumin), lipids (stearic acid, oleic acid, elaidic acid, and 1,2-decanediol), and carbohydrates (amylopectin, agarose, trehalose, and raffinose) representative of phytoplankton-derived organic matter.

2. METHODS

2.1. Chemical Representation. Chosen representative constituents of natural seawater are listed in Table 1. Representative inorganic components of SSA were NaCl (≥99.9%, Macron Chemical) and synthetic seawater (SSW; Paragon Scientific). SSW contains the major inorganic salts of natural seawater (NaCl, $MgCl_2$, KCl, $CaSO_4$, and $NaHCO_3$). Cultures of *Prochlorococcus* were used as model sources of marine organic carbon. Three strains of *Prochlorococcus* (MED4, MIT9312 and NATL2A, members of the HLI, HLII, and LLI clades, respectively) were grown as axenic cultures in a natural seawater based PRO99 medium amended with nutrients.[31,33] Cells were grown in a 13:11 light:dark

DOI: 10.1021/acs.est.8b05150
Environ. Sci. Technol. 2019, 53, 1139−1149

incubator at 24 °C, attaining average concentrations of 5×10^8 cells mL^{-1}. Despite these elevated concentrations, we do not expect the structure or composition of organic byproducts to be altered.[33] Some cell cultures were lysed by sonication for 5 min prior to aerosolization, while other cell cultures were not.

Single component organic particles were generated from various compounds chosen to mimic proteins, lipids, and saccharides found in natural SSA (Table 1).[18,34] Most organics were size selected at 200 nm diameter prior to ice nucleation analysis. Particles generated from lysed cells were also size selected at 500 nm and sampled polydisperse. The protein class was represented by bovine serum albumin (BSA; ≥ 99%, protease and fatty acid free), L-threonine (≥99%), L-arginine (≥99%), and L-aspartic acid (≥98). Lipids were represented by stearic acid (≥98.5%), oleic acid (≥99%), elaidic acid (≥98%, Acros Organics), and 1,2-decanediol (≥99%). Finally, the saccharides were represented by amylopectin (≥99%), D-(+)-trehalose (≥99%), D-(+)-raffinose (≥99%), and agarose (BioUltra ≥99.5%). Unless noted, chemical stocks were obtained from Sigma-Aldrich. Mixtures of each class contained equal proportions of components by mass.

2.2. Aerosolization. Solutions of inorganics, cell cultures, and single component organic compounds were aerosolized using a glass frit bubbler (Figure S1 of the Supporting Information, SI). We note the frit bubbler has been found to both artificially enrich and deplete aerosols in organic matter.[35,36] Filtered lab air free of particles larger than 10 nm in diameter was passed through a sintered glass frit with pore sizes between 4.0 and 5.5 μm at a flow rate of 0.20 L min^{-1}, resulting in bubble sizes between 0.015 and 9.5 mm in diameter (Figure S2). After generation, aerosols were dried to a relative humidity of 15% by passing the particle stream through three consecutive 43 cm diffusion dryers. Some samples were size selected using a differential mobility analyzer (DMA, Model 2002; Brechtel Manufacturing Inc., Hayward, CA) with a sheath to sample flow ratio of 8.0 (Figure S3). The sheath flow of the DMA was dried with desiccant to an RH of less than 10%.

Figure 1 illustrates ambient size distributions from the tropical South Atlantic Ocean,[37] the North Atlantic Ocean,[38] and the tropical North Pacific Ocean.[39] Up to 90% of Aitken mode (>110 nm diameter) particles in marine environments can be of secondary origin, and would not be replicated using the frit bubbler.[40] Also illustrated are this study's and another's size distributions from a frit bubbler. Note that although SSA has a significant size fraction above 1 μm,[41] we restrict our analysis to the submicrometer range due to size sampling constraints of our instrumentation. Our frit's size distributions generally demonstrate a bimodal size distribution with peaks at 200 nm (±88 nm) and 500 nm (±73 nm), with variability representing the average standard deviation about the mode. We tentatively assign these two modes as film burst and jet drop particle production, respectively. Additional details about bubble sizes, aerosol production, and flux[42] compared with other studies can be found in the SI.

2.3. Chemical Characterization. The Particle Analysis by Laser Mass Spectrometry (PALMS) instrument collected compositional information on a particle-by-particle basis. Aerosol particles were drawn into PALMS and collimated via an aerodynamic inlet. Particle diameters ranged between 0.2–1.5 μm.[43] The carrier gas is pumped away under vacuum, yet the residence time is short enough to minimize the loss of volatile organic components from the particulate surface.[44]

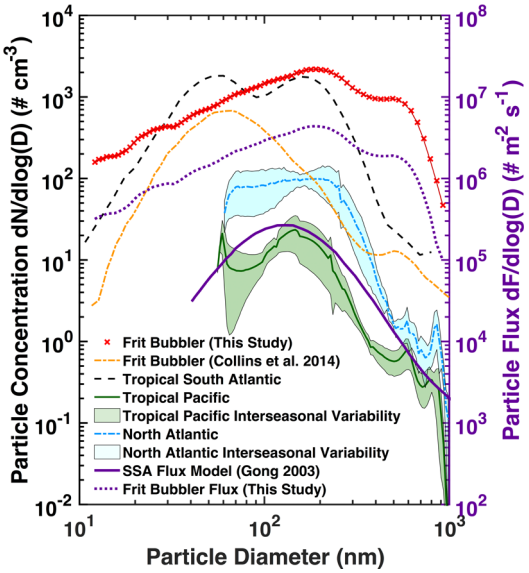

Figure 1. Submicrometer Aerosol Size Distributions (left axis) and Production Fluxes (purple lines; right axis). Laboratory and field size distributions show number concentrations of particles dN with diameters between D and D+dD. Frit bubbler data for this study are from synthetic seawater. Data from the Collins et al. 2014 frit bubbler, Tropical South Atlantic, North Atlantic, and the Tropical North Pacific are from sources 35, 37, 38, and 39, respectively. The particle flux model parametrization is from source 42 assuming a wind speed of 8 m s^{-1}.

Two continuous-wave 532 nm Nd:YAG laser beams spaced 34 mm apart measured particle velocity, which were converted to vacuum aerodynamic diameter.[43] Particles were then ionized using a 193 nm ultraviolet (UV) excimer laser. Atomic and molecular ions were accelerated in a reflectron before impacting a microchannel plate detector, allowing for an ion's time-of-flight to be converted to a mass to charge (m/z) ratio. Either a positive or a negative mass spectrum is acquired per particle. Particle ionization with the UV excimer is not quantitative, but ionization of most atmospherically relevant components can be demonstrated. The relative intensity of peaks in a mass spectrum may reflect the orientation of the particle relative to the UV laser beam, matrix effects, and different ionization efficiencies of different components.[45] To qualitatively compare the organic carbon content of compositionally similar particle assemblages, hundreds of particle spectra were collected for each sample in order to correct for these phenomena.

2.4. Ice Nucleation. The SPectrometer for Ice Nuclei (SPIN; Droplet Measurement Technologies, Boulder, CO) quantifies the nucleation efficiency of INPs.[46] SPIN consists of two flat parallel plates, separated by 1.0 cm and coated with 1.0 mm of ice, whose temperatures are controlled independently. The temperature and ice saturation ratio (S_{ice}) that the aerosol lamina experienced was controlled by varying the temperature gradient between the two walls. SPIN operated in a temperature ($-40 < T < -60$ °C) and supersaturation ($1.0 < S_{ice} < 1.5$) regime relevant to cirrus cloud formation. The lamina S_{ice} was raised isothermally at a rate of 0.02 per minute by increasing the wall temperature gradient to homogeneous nucleation, then lowered isothermally at an equal rate to ice saturation.[46] Due to slight heterogeneities in wall temperatures, the temperature and supersaturation in the SPIN aerosol

DOI: 10.1021/acs.est.8b05150
Environ. Sci. Technol. 2019, 53, 1139–1149

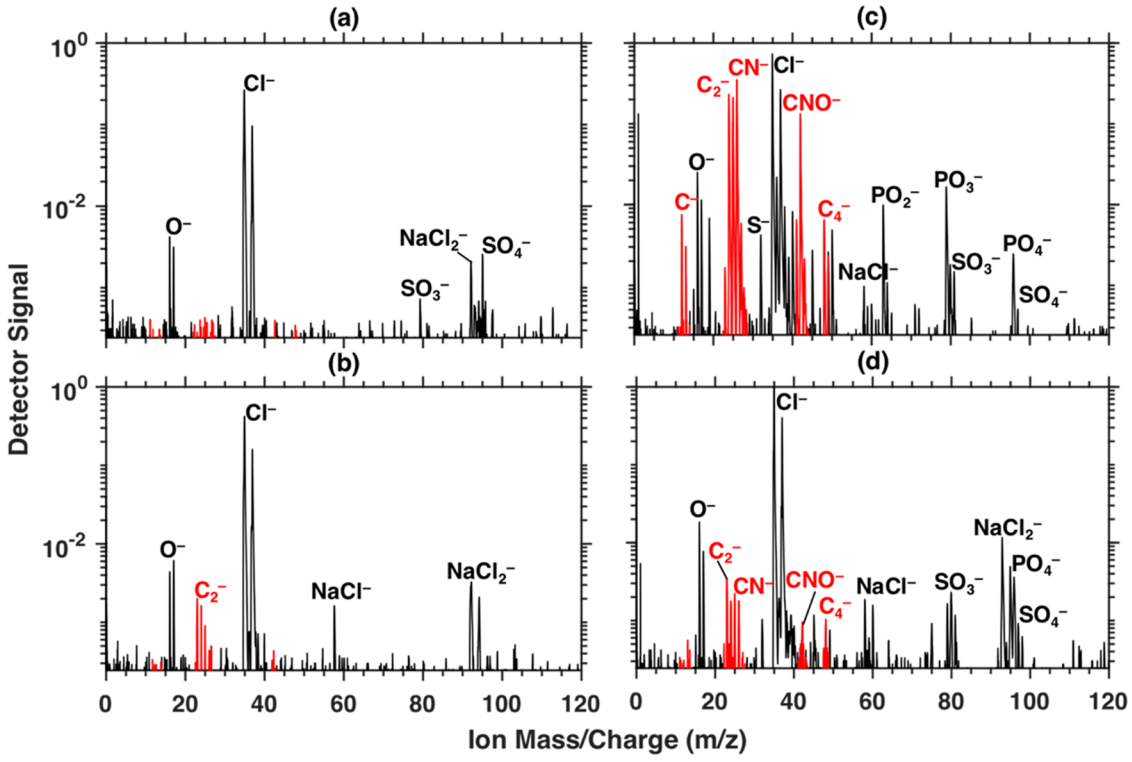

Figure 2. Particle mass spectra. Characteristic negative spectra are shown for (a) synthetic seawater particles (shown for a 200 nm particle), (b) *Prochlorococcus* culture medium particles (shown for a 200 nm particle), and (c) 200 nm and (d) 500 nm particles generated from a lysed *Prochlorococcus* (NATL2A) culture. Peaks associated with organic carbon ions are highlighted in red.

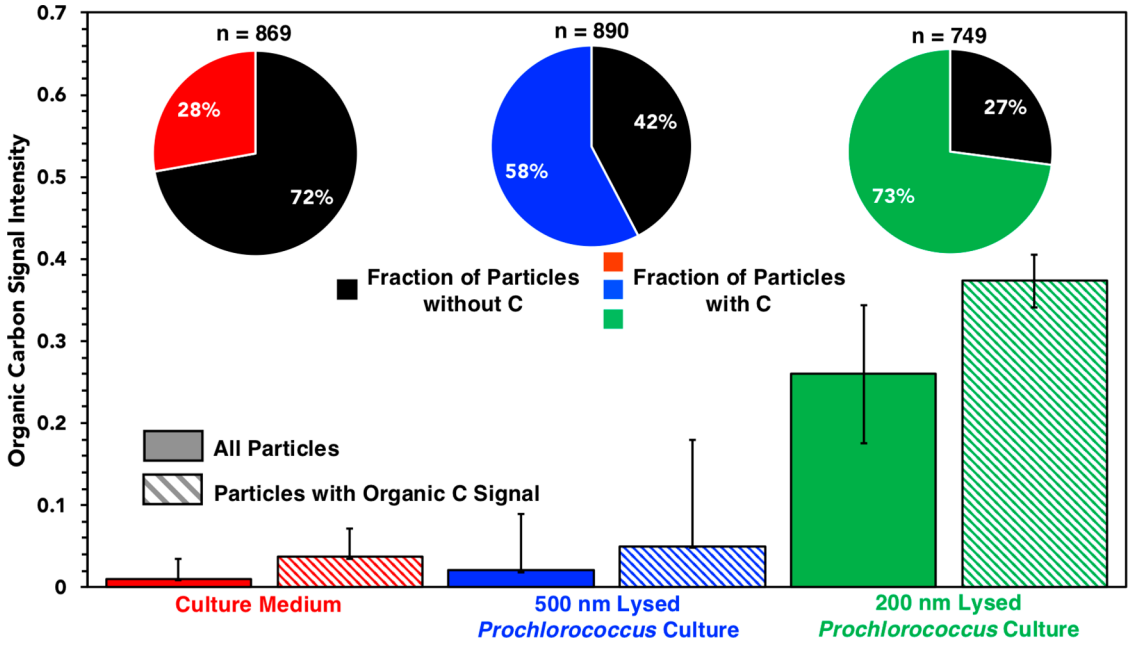

Figure 3. Average organic carbon signal intensity is shown for culture medium, 500 nm, and 200 nm particles from a lysed *Prochlorococcus* (NATL2A) culture. Organic carbon is defined as the sum of $C_wH_xO_yN_z$ peak integrals divided by total ion signal, with $1 \leq w \leq 4$ and $0 \leq x, y, z \leq 4$ in whole number increments. Signal intensity is shown for all particles of the same type and only particles exhibiting an organic carbon signal. Error bars represent one standard deviation in signal variability.

lamina vary. The uncertainty in the average lamina conditions can be calculated using thermocouple measurements on each wall.[47] Aerosol particles are fed into the chamber in a lamina flow of about 1.0 L min^{-1} supplemented with a sheath flow of about 9.0 L min^{-1}. However, turbulence at the inlet causes particles to spread outside the centerline lamina. We quantified the fraction of particles within the lamina over the conditions considered in this experiment (Figure S4). As particles outside the lamina experience a lower supersaturation and are less likely to activate, a correction factor between 1.86 and 7.96 is

DOI: 10.1021/acs.est.8b05150
Environ. Sci. Technol. 2019, 53, 1139−1149

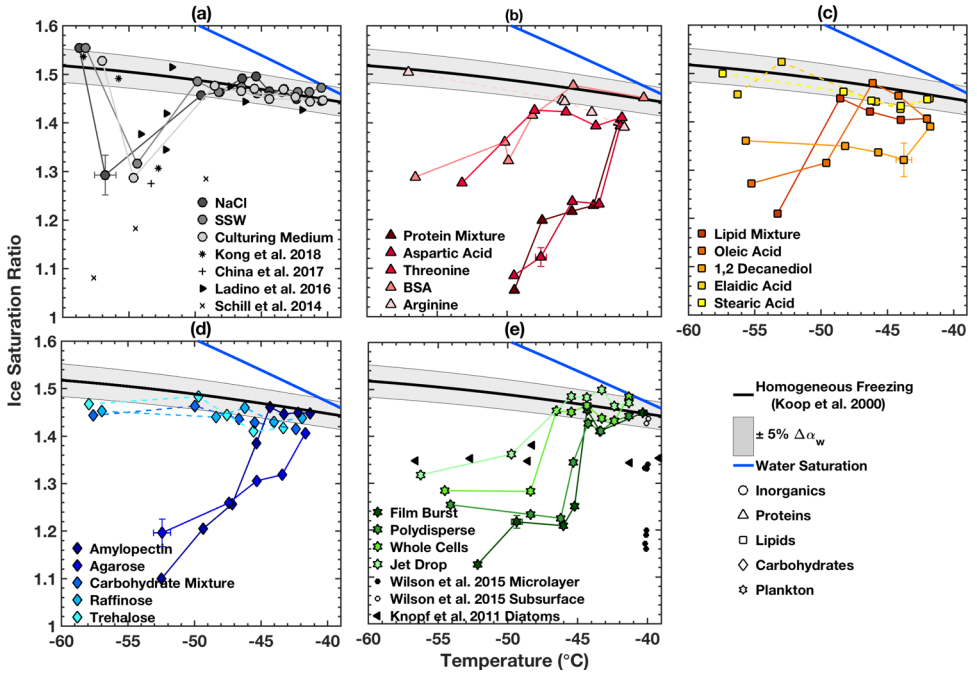

Figure 4. Ice supersaturation at the onset of ice nucleation is depicted for (a) inorganics and culturing media, (b) proteins, (c) lipids, (d) saccharides, and (e) *Prochlorococcus* cultures. The point of nucleation onset is defined as when 1 in 10^4 particles nucleate ice, correcting for spreading outside the SPIN lamina (Figure S4). Solid lines indicate substances nucleated heterogeneously, while dashed lines indicate nucleation was indistinguishable from homogeneous nucleation (Koop et al. 2000; Source 82) due to uncertainty in SPIN lamina conditions.[45] Data points represent the average of two or more replicate experiments. Representative error bars indicate a standard deviation of certainty in the SPIN aerosol lamina conditions

applied to fractional activation data derived assuming all particles are constrained to the lamina.[48,49]

An optical particle counter collected side scatter and laser light depolarization data on a particle-by-particle basis (Figure S5). Activated particles between 0.50 and 15 μm were detected. A machine learning algorithm was then trained using four optical parameters to categorize particles by phase.[46] Fractional activation was calculated by dividing ice concentrations assigned by the machine learning output to total particle concentrations measured by a condensation particle counter (CPC, Model 1700; Brechtel Manufacturing Inc., Hayward, CA) running in parallel to SPIN. For SPIN experiments on polydisperse particle streams, an impactor with a 1 μm diameter cutoff was used.

Frost occasionally sheds from the iced walls, contributing to a background ice particle concentration. With proper SPIN setup, a background of less than 10 per L of sample air can be achieved.[46] This is below the threshold ice concentration used to determine the onset of ice nucleation for all experiments considered here (see the SI section for a derivation of this detection limit).

3. RESULTS AND DISCUSSION

3.1. Chemical Interpretation of Sea Spray Aerosol. Representative negative PALMS spectra are shown for SSW, PRO99 culture medium, and 200 and 500 nm particles generated from a lysed culture of *Prochlorococcus* in Figure 2. Red peaks indicate the detector signal from organic carbon signatures. The SSW spectrum exhibits inorganic ion peaks expected from seawater excimer fragmentation, including two isotopes of chlorine (m/z = 35 and 37) and clusters of sodium and chlorine. The oxygen ions may result from gaseous adsorption to the particle surface within the vacuum. The culturing medium shows a weak carbon signature, potentially from the added organic chelating agent EDTA.[33] Spectra from 200 nm particles aerosolized from lysed *Prochlorococcus* (NATL2A) cultures typically exhibit robust organic carbon signals. Organic nitrogen (CN^- m/z = 26 and CNO^- m/z = 42) may result from the ionization of amine functional groups, and the phosphorus signals (PO_2^- m/z = 63; PO_3^- m/z = 79; and PO_4^- m/z = 95) may result from the ionization of phospholipids or from phosphate backbones of nucleic acids. 500 nm particles aerosolized from the same lysed culture exhibit a lower organic carbon, nitrogen, and phosphorus signal. The oxygen and hydroxyl signals (m/z = 16 and 17) in lysed cell culture spectra are enhanced relative to the SSW and culturing medium spectra. This may be due the ionization of carboxyl and hydroxyl functional groups.

The average organic carbon signals across hundreds of negative mass spectra for three aerosol types are shown in Figure 3. Organic carbon is defined as the integral-sum of $C_wH_xO_yN_z$ peaks divided by total ion signal, where $1 \leq w \leq 4$ and $0 \leq x, y, z \leq 4$. Peaks known to coincide with inorganic signatures are excluded. The fraction of particles exhibiting an organic carbon signal and the average signal for particles exhibiting organic carbon signatures are also shown in Figure 3. The aerosolized culturing medium produced the fewest carbon containing particles between the three samples, followed by 500 nm and then 200 nm particles from lysed *Prochlorococcus* cultures. The mean organic carbon signal for the culturing medium is statistically lower at the 99% confidence interval than that of the 500 nm lysed cell culture particles ($p = 4.1 \times 10^{-7}$). The 500 nm lysed cell culture particles in turn exhibit a lower organic carbon signal than the 200 nm lysed cell culture particles ($p = 1.1 \times 10^{-148}$). We also measured the organic content of polydisperse particles

DOI: 10.1021/acs.est.8b05150
Environ. Sci. Technol. 2019, 53, 1139−1149

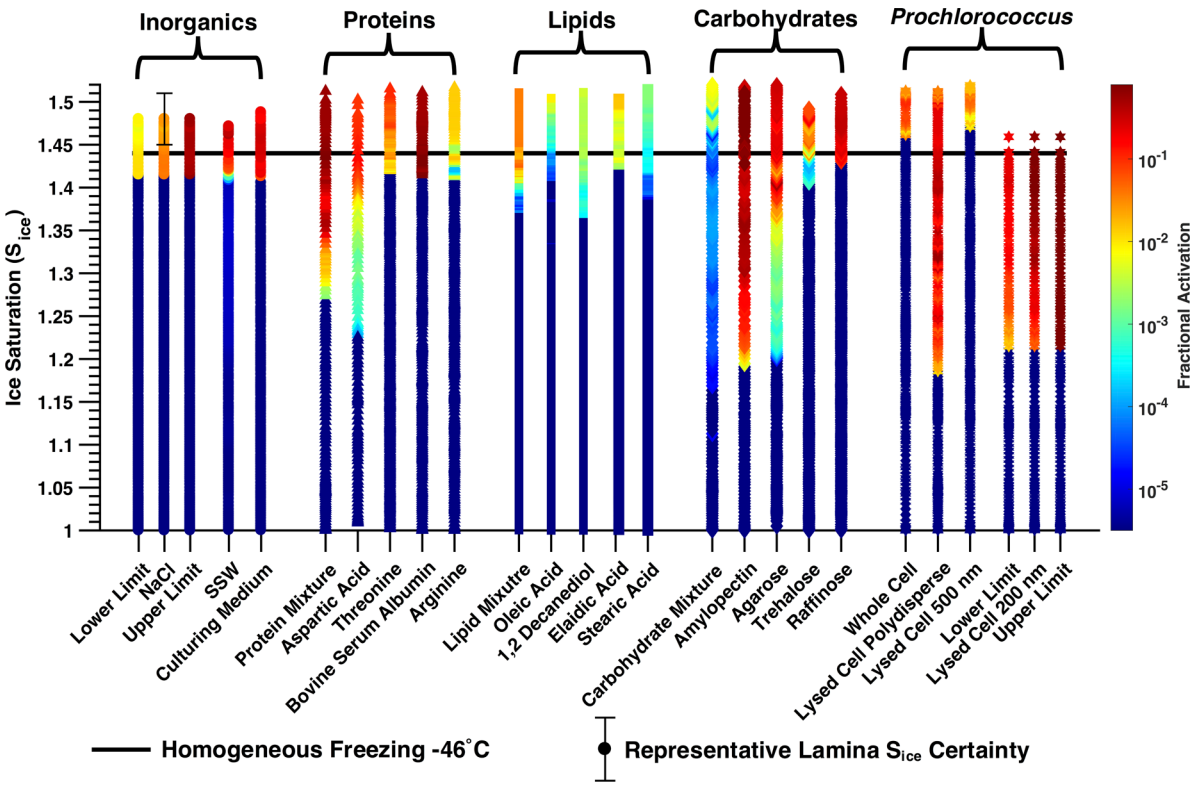

Figure 5. Fraction of particles activated as a function of ice saturation is depicted for experiments run at −46 °C. Fractional activation is corrected for aerosol spreading outside the SPIN lamina (Figure S4). Also illustrated are the onset point for homogeneous nucleation (Source 82) and a standard deviation of variability in SPIN aerosol lamina saturation at −46 °C. The effects of correction factor uncertainty is illustrated for NaCl and 200 nm particles from lysed *Prochlorococcus* cultures.

generated from whole *Prochlorococcus* cultures. *Prochlorococcus* cells are small enough (500−700 nm) where they can be sampled with PALMS. However, these spectra show very little organic signal relative to the lysed cell culture particles (0.01 + 0.005/−0.002, with uncertainties representing a standard deviation above and below the mean). We therefore conclude that whole cells were not efficiently aerosolized with the bubbler.

We hypothesize that this compositional disparity results from differing mechanisms of aerosol particle formation. The culturing medium contains a dilute fraction of soluble organics[33] which are aerosolized and ionized along with inorganic salts to yield a weak organic carbon signal. The 200 nm particles aerosolized from lysed *Prochlorococcus* cultures could be organically enriched because they are aerosolized from organically-enriched films of bubbles, a hypothesis supported by previous studies.[50−52] The larger 500 nm SSA particles could then exhibit a lower organic signal because they are generated from subsurface water via the jet drop production mechanism.[53] These results indicate that the ice nucleation efficiency of SSA may be size dependent, with smaller organically enriched particles nucleating at lower ice supersaturations than larger inorganic particles.

3.2. Depositional Ice Nucleation Onset. The ice saturation at the onset of ice nucleation—termed critical supersaturation—for inorganic, protein, lipid, saccharide, and *Prochlorococcus* culture particles is shown in Figure 4. The onset of ice nucleation is defined as one in 10^4 particles activating for a period of 10 s after correcting for aerosol spreading outside the lamina (Figure S4). Each data point represents the average onset conditions of at least two replicate experiments. Representative error bars indicate a standard deviation of uncertainty in SPIN lamina conditions.[47]

No group of particles with similar chemistry exhibited uniform temperatures and supersaturations at the onset of ice nucleation. All substances nucleated homogeneously above −43 °C. Particles generated from NaCl, synthetic seawater, and culturing medium activated homogeneously until heterogeneous nucleation initiated around −55 °C (Figure 4a). Below −58 °C, these particles again nucleated homogeneously. This pattern is likely due to the kinetic competition between depositional nucleation and deliquescence, the latter of which leads to homogeneous freezing.[11,54] These results agree with previous studies that found marine derived inorganics to be moderately effective to poor depositional INPs at temperatures below −50 °C.[8−11]

The critical S_{ice} of some pure organic compounds decreased at colder temperatures (Figure 4b−d). Aspartic acid likely determined the nucleation behavior of the protein mixture, which initiated nucleation at an S_{ice} of 1.04 at −50 °C (Figure 4b). Threonine and BSA nucleated at moderate (1.27−1.36) ice supersaturations below −50 °C. Arginine nucleated homogeneously across all temperatures. Amylopectin and agarose were effective heterogeneous INPs at temperatures below −46 °C, while the smaller saccharides trehalose and raffinose nucleated homogeneously across all temperatures (Figure 4d). The saccharide mixture nucleated homogeneously as well. On average, the critical S_{ice} of lipids exhibited the weakest response to temperature (Figure 4c). The lipid mixture and 1,2-decanediol exhibited a modest decrease in critical S_{ice}, nucleating at an S_{ice} of 1.21 and 1.27 around −54 °C and −56 °C, respectively.

DOI: 10.1021/acs.est.8b05150
Environ. Sci. Technol. 2019, 53, 1139−1149

The onset of ice nucleation was characterized for two to three strains of *Prochlorococcus* and averaged at each temperature (Figure 4e). Particles aerosolized from whole cell cultures nucleated homogeneously until −48 °C, below which they nucleated depositionally near an S_{ice} of 1.28. 500 nm particles aerosolized from lysed *Prochlorococcus* cultures and size selected using the DMA exhibited a weak critical S_{ice} response to temperature, likely due to the deliquescence of their inorganic components. These particles nucleated homogeneously until −49 °C, below which they likely nucleated in the deposition or deliquescent freezing modes[55] between an S_{ice} of 1.32 and 1.36. Polydisperse and 200 nm particles aerosolized from lysed *Prochlorococcus* cultures nucleated heterogeneously below −44 °C. The 200 nm particles in particular were very effective heterogeneous INPs, nucleating at an S_{ice} of 1.12 below −50 °C. The 200 nm particles within the polydisperse stream likely determined the critical S_{ice} of the polydisperse aerosol assemblage, as these two samples exhibited statistically indistinguishable critical S_{ice} within two standard deviations of uncertainty (95% confidence intervals) in SPIN lamina conditions between −40 °C and −50 °C. These results expand upon previous findings, which found that aerosolized samples of the North Atlantic microlayer nucleated at a warmer temperature of −40 °C but at an S_{ice} comparable to the 200 nm lysed *Prochlorococcus* particles.[23] Another study demonstrated that exudates from the diatom *T. pseudonana* exhibited a higher critical S_{ice} than our *Prochlorococcus* particles between −44 °C and −60 °C.[28]

The smaller particles generated from lysed *Prochlorococcus* are likely more effective INPs because they are organically enriched (Figure 3). On the basis of previous studies, we speculate that these organic substances may provide a hydrogen-bonding template to lower the activation energy of ice nucleation. Amylopectin, agarose, and aspartic acid exhibited critical supersaturation-temperature responses (3.5, 1.8, and 3.7% S_{ice} K^{-1}, respectively), that most closely mimicked the slope of 200 nm lysed *Prochlorococcus* particles (3.0% S_{ice} K^{-1}). These polysaccharides and proteinaceous molecules have multiple hydrogen bonding moieties, specifically hydroxyl groups. Molecular modeling on known INPs suggests hydroxyl groups hydrogen bond with water molecules and align them into a critical ice embryo,[56] which may explain the effectiveness of amylopectin and agarose as depositional INPs. Incompatible hydroxyl orientation can hinder nucleation by inhibiting the growth of an ice crystal embryo sufficiently large to overcome the free energy of nucleation.[57,58] This may explain why some hydrogen bond forming molecules, such as threonine, arginine, and BSA, are ineffective INPs. Substances that deliquesce or adsorb water are also precluded from depositionally nucleating. Although the hygroscopic growth of raffinose and trehalose is not reported in the literature, many oligosaccharides readily adsorb water vapor on their surface.[59,60] This process forms a thin film of liquid water that prevents ice deposition on the particulate surface.

3.3. Fractional Activation. Ice nucleation initiates at a critical supersaturation followed by a generally increasing fractional activation as S_{ice} rises (Figure 5). Another graphical representation of this data is depicted in Figure S6. We chose to depict fractional activation at −46 °C because this was warmest temperature at which at least one compound from each organic class nucleated heterogeneously. Although average SPIN ice backgrounds are subtracted from the fractional ice activation data, occasional frost shedding from the SPIN ice walls can sometimes temporarily increase the apparent fractional activation.[46] The reported fractional activation takes into account the correction factor derived from Figure S4. Inorganics show no activation until homogeneous freezing is reached (S_{ice} = 1.42). Nearly 100% of hygroscopic particles nucleate ice in the homogeneous freezing regime when the upper limit of fractional activation, derived from the upper correction factor, is applied. Aspartic acid is the only amino acid or protein exhibiting heterogeneous nucleation at this temperature, initiating nucleation at an S_{ice} of 1.22. Lipids are ineffective INPs, with 1,2-decanediol and stearic acid exhibiting a high S_{ice} at onset (1.35 and 1.39, respectively). Agarose and amylopectin exhibited a low critical S_{ice}, initiating activation at 1.17 and 1.19, respectively. The critical S_{ice} and fractional activation of mixtures generally resembled those of their most effective component. Mixed carbohydrate particles, however, exhibited lower fractional activation likely due to the deliquescence of raffinose and trehalose. These deliquesced particles would be precluded from undergoing depositional ice nucleation. Finally, polydisperse and size-selected 200 nm particles from lysed *Prochlorococcus* cultures were effective depositional ice nuclei, activating at a low S_{ice} and reaching the highest fractional activation (f_{act} = 0.1) of all tested substances.

The fractional activation for organically enriched 200 nm *Prochlorococcus* particles most closely matches the fractional activation for amylopectin and agarose. These three substances exhibit a rapid increase in fractional activation once their respective critical S_{ice} are reached. This phenomenon has been observed for several organic aerosol systems, indicating that particles of these substances may be relatively uniform in factors that affect ice nucleation efficiency, such as composition or surface morphology.[14,61,62]

Interpreting the fractional activation data reveals that polysaccharides and proteins may be important in determining the ice nucleation efficiency of SSA, whereas lipids are generally ineffective depositional INPs under the considered conditions. One factor that may explain the INP ability of these substances is their phase state. Studies have indicated that organic particles can undergo glassy phase transitions that affect their ice nucleation efficiency.[63,64] We have calculated the glass transition temperature (T_g) of single component organic compounds based on DeRieux et al. 2018.[65] The T_g values are listed in Table 1 at three relative humidities with respect to water (RH_w). Note that 70% RH_w approximately corresponds to S_{ice} = 1.0, whereas 90% RH_w approximately corresponds to homogeneous freezing in the considered temperature range.

Aspartic acid, amylopectin, and agarose all exhibit T_g values at or well above the conditions considered in this study. This indicates that these particles are sufficiently viscous to prevent full deliquescence, which may explain their ability to nucleate heterogeneously in this regime. 1,2-Decanediol has the lowest T_g of the lipid-like compounds, yet also exhibited the lowest average critical supersaturation among the lipids between −42 °C and −56 °C. Trehalose and raffinose are also glassy at these conditions, yet do not depositionally nucleate. Glassy phase transitions can therefore not fully explain the depositional nucleation ability of all tested organic compounds. One reason may be that the particles do not fully undergo glassy state phase transitions due to the short time scales over which particles experience a change in RH and temperature upon entering SPIN.

DOI: 10.1021/acs.est.8b05150
Environ. Sci. Technol. 2019, 53, 1139−1149

A second factor that may explain the ice nucleation ability of certain compounds is their capability to hydrogen bond with and retain water molecules in the initial critical ice embryo. Among the tested amino acids, aspartic acid has the most amine and carboxylic acid groups that can act as hydrogen bond donors. Agarose and amylopectin both form helical structures that order thousands of hydroxyl moieties per molecule.[66] This suggests organic molecules with large numbers of hydrogen bonding sites may provide a template able to initiate ice embryo formation.[67,68] These substances may therefore be more effective depositional INPs than molecules lacking the requisite chemistry. Not all molecules with hydrophilic functional groups nucleated heterogeneously. Trehalose, raffinose, threonine, arginine, and BSA did not exhibit heterogeneous ice nucleation behavior. To nucleate ice in deposition mode, particles must not absorb liquid water, and the orientation of the hydrogen bonding template must match the crystallographic structure of ice.[56]

3.4. Environmental Implications. Chemical analysis of ice residuals from marine cirrus indicates a substantial fraction of ice residuals bear SSA signatures.[27] Our results suggest that select organic components of SSA may be a source of efficient INPs for cirrus ice nucleation. To further investigate the similarities in ice nucleation efficiency between pure organic components and *Prochlorococcus* derived particles, we calculated the ice nucleation active site densities (n_S) for each size selected compound by dividing activated INP concentration (n_i) by surface area concentration (s_a):

$$n_S = \frac{n_i}{s_A} = \frac{f_{ice}}{s_a} \quad (1)$$

where f_{ice} is fractional activation, and s_a is the surface area of a single particle. To describe n_S as a function of a single variable, temperature (in K) and S_{ice} are combined into a single thermodynamic variable x_{therm}:

$$x_{therm} = (273.15 - T) + (S_{ice} - 1) \times 100 \quad (2)$$

Values of $n_S(T, S_{ice})$ as a function of x_{therm} for single component and *Prochlorococcus* derived particles are detailed in the SI. Those compounds which most closely matched the $n_S(T, S_{ice})$ values for 200 nm lysed culture particles were aspartic acid, 1,2-decanediol, and amylopectin from the protein, lipid, and carbohydrate classes, respectively (Figure S7). Our analysis demonstrates that the organic components of SSA bear comparable n_S values to other common INPs, such as soil and mineral dusts under the considered conditions (Figure 6).[69−73] However, we note that our choice of aerosolization technique may have produced organically enriched particles relative to natural SSA, so we caution that the n_S isoline in Figure 6 may depict a lower estimate of S_{ice}.

These results suggest that the depositional ice nucleation efficiency of natural SSA may be determined by the presence of hydrophilic and macromolecular compounds found in in the marine microlayer. Likely candidates include polysaccharides, lipopolysaccharides, and proteins.[50,74,75] Our results also suggest that events which enrich the sea surface organic microlayer, such as phytoplankton blooms and subsequent cell lysis by predation, may transiently increase emission rates of SSA INPs.[76] Furthermore, these results highlight a potential shortcoming of parametrizations that use surface chlorophyll concentrations as a predictor of SSA organic mass fraction and INP efficiency.[77−79] In oligotrophic regions where *Prochlorococcus* dominates, surface chlorophyll abundance is a poor indicator of aerosol organic carbon content because most carbon fixation occurs at depths greater than those retrievable by satellite sensors.[80] Organic matter is transported from these depths to the surface by eddy diffusion, wave breaking, and bubble scavenging.[23,80,−82]

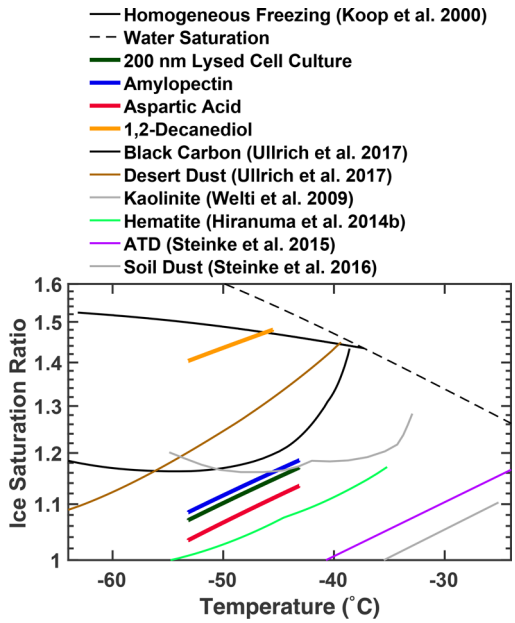

Figure 6. Comparison of ice nucleation active site density parametrizations for 200 nm lysed *Prochlorococcus* culture particles, amylopectin, aspartic acid, 1,2-decanediol, black carbon, and desert dust (Ullrich et al. 2017; source 69), Kaolinite (Welti et al. 2009; Source 70), hematite (Hiranuma et al. 2014b; Source 71), Arizona test dust (ATD; Steinke et al. 2015; Source 72), and soil dust (Steinke et al. 2016; Source 73). For clarity, only the $n_S = 10^{10}$ m^{-2} isolines are illustrated and uncertainties are omitted. Uncertainties in this study's parametrizations can be derived from Figure S7.

Further research should isolate polysaccharides and proteins from natural seawater samples to confirm the ice nucleation abilities of these components. These data will establish how the nucleation efficiency of SSA may respond to factors that affect organic composition and stoichiometry like ocean eutrophication, stratification, acidification, and temperature change. We hypothesize that the changing chemical composition of marine aerosol particles may affect their depositional ice nucleation ability.

■ ASSOCIATED CONTENT

Supporting Information

The Supporting Information is available free of charge on the ACS Publications website at DOI: 10.1021/acs.est.8b05150.

An experimental schematic and the methods used to aerosolize solutions to quantify aerosol spreading outside of the SPIN lamina; Figure S1, flowchart of aerosol generation and measurements; Figure S2, bubble size distribution produced by this study's frit bubbler; Figure S3, size distribution of aerosol particles prior to size selection, when applicable; S4, the fraction of particles constrained to the lamina under experimental conditions considered in this study; Figure S5, an example of particle growth as a function of relative humidity after ice nucleation onset; Figure S6, fractional activation as a function of ice supersaturation; and

DOI: 10.1021/acs.est.8b05150
Environ. Sci. Technol. 2019, 53, 1139−1149

Figure S7, derivation of ice nucleation active site density parametrizations for select compounds (PDF)

AUTHOR INFORMATION

Corresponding Author

*Phone: 617 324 4882. E-mail: djcziczo@mit.edu.

ORCID

Martin J. Wolf: 0000-0002-8553-8808

Notes

The authors declare no competing financial interest.

ACKNOWLEDGMENTS

We would like to thank the M.I.T. David P. Bacon Fund for financial support. A.C., K.D., S.J.B., and S.W.C. were supported in part by NSF grant #OCE-1356460 to S.W.C., grants from the Simons Foundation (Life Sciences Project Award ID 337262, S.W.C; SCOPE Award ID 329108, S.W.C), and the Gordon and Betty Moore Foundation (Grant IDs GBMF495 and GBMF4511 to S.W.C.).

REFERENCES

(1) Stocker, T. F.; Qin, D.; Plattner, G.-K.; Tignor, M.; Allen, S. K. J.; Boschung, A.; Nauels, Y.; Xia, V. *Climate Change 2013 The Physical Science Basis Working Group I Contribution to the Fifth Assessment Report of the Intergovernmental Panel on Climate Change Summary for Policymakers*; Cambridge University Press: Cambridge/New York, 2013, p 33.

(2) Albrecht, B. A. Aerosols, Cloud Microphysics, and Fractional Cloudiness. *Science* **1989**, *245* (4923), 1227−1230.

(3) Hansen, J.; Sato, M.; Ruedy, R. Radiative Forcing and Climate Response. *J. Geophys. Res. Atmos.* **1997**, *102* (D6), 6831−6864.

(4) Rossow, W. B.; Schiffer, R. A. Advances in Understanding Clouds from ISCCP. *Bull. Am. Meteorol. Soc.* **1999**, *80* (11), 2261−2287.

(5) Twomey, S. The Influence of Pollution on the Shortwave Albedo of Clouds. *J. Atmos. Sci.* **1977**, *34* (7), 1149−1152.

(6) Pruppacher, H. R.; Klett, J. D. *Microphysics of Clouds and Precipitation*: *Reprinted 1980*; Springer Science & Business Media, 1980.

(7) Gasparini, B.; Meyer, A.; Neubauer, D.; Münch, S.; Lohmann, U. Cirrus Cloud Properties as Seen by the CALIPSO Satellite and ECHAM-HAM Global Climate Model. *J. Clim.* **2018**, *31* (5), 1983−2003.

(8) China, S.; Alpert, P. A.; Zhang, B.; Schum, S.; Dzepina, K.; Wright, K.; Owen, R. C.; Fialho, P.; Mazzoleni, L. R.; Mazzoleni, C.; Knopf, D. A. Ice Cloud Formation Potential by Free Tropospheric Particles from Long-Range Transport over the Northern Atlantic Ocean. *J. Geophys. Res. Atmos.* **2017**, *122* (5), 3065−3079.

(9) Ladino, L. A.; Yakobi-Hancock, J. D.; Kilthau, W. P.; Mason, R. H.; Si, M.; Li, J.; Miller, L. A.; Schiller, C. L.; Huffman, J. A.; Aller, J. Y.; Knopf, D. A.; Bertram, A. K.; Abbatt, J. P. D. Addressing the Ice Nucleating Abilities of Marine Aerosol: A Combination of Deposition Mode Laboratory and Field Measurements. *Atmos. Environ.* **2016**, *132*, 1−10.

(10) Schill, G. P.; Tolbert, M. A. Heterogeneous Ice Nucleation on Simulated Sea-Spray Aerosol Using Raman Microscopy. *J. Phys. Chem. C* **2014**, *118* (50), 29234−29241.

(11) Kong, X.; Wolf, M. J.; Roesch, M.; Thomson, E. S.; Bartels-Rausch, T.; Alpert, P. A.; Ammann, M.; Prisle, N. L.; Cziczo, D. J. A Continuous Flow Diffusion Chamber Study of Sea Salt Particles Acting as Cloud Nuclei: Deliquescence and Ice Nucleation. *Tellus, Ser. B* **2018**, *70* (1), 1463806.

(12) Adler, G.; Koop, T.; Haspel, C.; Taraniuk, I.; Moise, T.; Koren, I.; Heiblum, R. H.; Rudich, Y. Formation of Highly Porous Aerosol Particles by Atmospheric Freeze-Drying in Ice Clouds. *Proc. Natl. Acad. Sci. U. S. A.* **2013**, *110* (51), 20414−20419.

(13) Cox, S. J.; Kathmann, S. M.; Slater, B.; Michaelides, A. Molecular Simulations of Heterogeneous Ice Nucleation. I. Controlling Ice Nucleation through Surface Hydrophilicity. *J. Chem. Phys.* **2015**, *142* (18), 184704.

(14) Wagner, R.; Möhler, O.; Saathoff, H.; Schnaiter, M.; Skrotzki, J.; Leisner, T.; Wilson, T. W.; Malkin, T. L.; Murray, B. J. Ice Cloud Processing of Ultra-Viscous/Glassy Aerosol Particles Leads to Enhanced Ice Nucleation Ability. *Atmos. Chem. Phys.* **2012**, *12*, 8589−8610.

(15) Azam, F.; Malfatti, F. Microbial Structuring of Marine Ecosystems. *Nat. Rev. Microbiol.* **2007**, *5* (10), 782−791.

(16) Bertilsson, S.; Berglund, O.; Pullin, M. J.; Chisholm, S. W. Release of Dissolved Organic Matter by *Prochlorococcus*. *Vie Milieu* **2005**, *55*, 3−4.

(17) Braakman, R.; Follows, M. J.; Chisholm, S. W. Metabolic Evolution and the Self-Organization of Ecosystems. *Proc. Natl. Acad. Sci. U. S. A.* **2017**, *114* (15), E3091−E3100.

(18) Biller, S. J.; Schubotz, F.; Roggensack, S. E.; Thompson, A. W.; Summons, R. E.; Chisholm, S. W. Bacterial Vesicles in Marine Ecosystems. *Science* **2014**, *343* (6167), 183−186.

(19) Garrett, W. D. The Organic Chemical Composition of the Ocean Surface. *Deep-Sea Res. Oceanogr. Abstr.* **1967**, *14* (2), 221−227.

(20) McCarthy, M.; Hedges, J.; Benner, R. Major Biochemical Composition of Dissolved High Molecular Weight Organic Matter in Seawater. *Mar. Chem.* **1996**, *55* (3−4), 281−297.

(21) McCarthy, M. D.; Hedges, J. I.; Benner, R. The Chemical Composition of Dissolved Organic Matter in Seawater. *Chem. Geol.* **1993**, *107* (3−4), 503−507.

(22) O'Dowd, C. D.; de Leeuw, G. Marine Aerosol Production: A Review of the Current Knowledge. *Philos. Trans. R. Soc., A* **2007**, *365* (1856), 1753−1774.

(23) Wilson, T. W.; Ladino, L. A.; Alpert, P. A.; Breckels, M. N.; Brooks, I. M.; Browse, J.; Burrows, S. M.; Carslaw, K. S.; Huffman, J. A.; Judd, C.; Kilthau, W. P.; Mason, R. H.; McFiggans, G.; Miller, L. A.; Nájera, J. J.; Polishchuk, E.; Rae, S.; Schiller, C. L.; Si, M.; Temprado, J. V.; Whale, T. F.; Wong, J. P. S.; Wurl, O.; Yakobi-Hancock, J. D.; Abbatt, J. P. D.; Aller, J. Y.; Bertram, A. K.; Knopf, D. A.; Murray, B. J. A Marine Biogenic Source of Atmospheric Ice-Nucleating Particles. *Nature* **2015**, *525* (7568), 234−238.

(24) Blanchard, D. C. The Electrification of the Atmosphere by Particles from Bubbles in the Sea. *Prog. Oceanogr.* **1963**, *1*, 73−202.

(25) Resch, F. *Oceanic Air Bubbles as Generators of Marine Aerosols*; Springer: Dordrecht, 1986; pp 101−112.

(26) Wang, X.; Deane, G. B.; Moore, K. A.; Ryder, O. S.; Stokes, M. D.; Beall, C. M.; Collins, D. B.; Santander, M. V.; Burrows, S. M.; Sultana, C. M.; Prather, K. A.; et al. Microbial Control of Sea Spray Aerosol Composition: A Tale of Two Blooms. *ACS Cent. Sci.* **2015**, *1* (3), 124−131.

(27) Cziczo, D. J.; Froyd, K. D.; Hoose, C.; Jensen, E. J.; Diao, M.; Zondlo, M. A.; Smith, J. B.; Twohy, C. H.; Murphy, D. M. Clarifying the Dominant Sources and Mechanisms of Cirrus Cloud Formation. *Science* **2013**, *340* (6138), 1320−1324.

(28) Knopf, D. A.; Alpert, P. A.; Wang, B.; Aller, J. Y. Stimulation of Ice Nucleation by Marine Diatoms. *Nat. Geosci.* **2011**, *4* (2), 88−90.

(29) Fletcher, N. H. Active Sites and Ice Crystal Nucleation. *J. Atmos. Sci.* **1969**, *26* (6), 1266−1271.

(30) Kanji, Z. A.; Ladino, L. A.; Wex, H.; Boose, Y.; Burkert-Kohn, M.; Cziczo, D. J.; Krämer, M.; Kanji, Z. A.; Ladino, L. A.; Wex, H.; Boose, Y.; Burkert-Kohn, M.; Cziczo, D. J.; Krämer, M. Overview of Ice Nucleating Particles. *Meteorol. Monogr.* **2017**, *58*, 1.1−1.33.

(31) Biller, S. J.; Berube, P. M.; Lindell, D.; Chisholm, S. W. *Prochlorococcus*: The Structure and Function of Collective Diversity. *Nat. Rev. Microbiol.* **2015**, *13*, 13−24.

(32) Flombaum, P.; Gallegos, J. L.; Gordillo, R. a; Rincón, J.; Zabala, L. L.; Jiao, N.; Karl, D.; Li, W.; Lomas, M.; Veneziano, D.; Vera, C.; Vrugt, J. A.; Martiny, A. C. Present and Future Global Distributions of the Marine Cyanobacteria *Prochlrococcus* and *Synechococcus*. *Proc. Natl. Acad. Sci. U. S. A.* **2013**, *110* (24), 9824−9829.

DOI: 10.1021/acs.est.8b05150
Environ. Sci. Technol. 2019, 53, 1139−1149

(33) Moore, L. R.; Coe, A.; Zinser, E. R.; Saito, M. a.; Sullivan, M. B.; Lindell, D.; Frois-Moniz, K.; Waterbury, J.; Chisholm, S. W. Culturing the Marine Cyanobacterium *Prochlorococcus*. *Limnol. Oceanogr.: Methods* **2007**, *5* (10), 353−362.
(34) Hicks, G. R.; Hironaka, C. M.; Dauvillee, D.; Funke, R. P.; D'Hulst, C.; Waffenschmidt, S.; Ball, S. G. When Simpler Is Better. Unicellular Green Algae for Discovering New Genes and Functions in Carbohydrate Metabolism. *Plant Physiol.* **2001**, *127* (4), 1334−1338.
(35) Collins, D. B.; Zhao, D. F.; Ruppel, M. J.; Laskina, O.; Grandquist, J. R.; Modini, R. L.; Stokes, M. D.; Russell, L. M.; Bertram, T. H.; Grassian, V. H.; Deane, G. B.; Prather, K. A. Direct Aerosol Chemical Composition Measurements to Evaluate the Physicochemical Differences between Controlled Sea Spray Aerosol Generation Schemes. *Atmos. Meas. Tech.* **2014**, *7* (11), 3667−3683.
(36) Long, M. S.; Keene, W. C.; Kieber, D. J.; Frossard, A. A.; Russell, L. M.; Maben, J. R.; Kinsey, J. D.; Quinn, P. K.; Bates, T. S. Light-Enhanced Primary Marine Aerosol Production from Biologically Productive Seawater. *Geophys. Res. Lett.* **2014**, *41* (7), 2661−2670.
(37) Koponen, I. K.; Virkkula, A.; Hillamo, R.; Kerminen, V. M.; Kulmala, M. Number Size Distributions and Concentrations of Marine Aerosols: Observations during a Cruise between the English Channel and the Coast of Antarctica. *J. Geophys. Res.* **2002**, *107* (24), 1−8.
(38) Atmospheric Radiation Measurement (ARM) Climate Research Facility, Ultrahigh Senstitivty Aerosol Spectrometer, Jan. 2014−Dec. 2014, 39° 5′ 29.76″ N, 28° 1′ 32.52″ W: Eastern North Atlantic Facility ARM Data Archive, Graciosa Island, Azores, Portugal.
(39) Lewis, E. R.; Wiscombe, W. J.; Albrecht, B. A.; Flagg, C. N.; Reynolds, R. M.; Siebesma, A. P. MAGIC: Marine ARM GPCI Investigation of Clouds. **2012**, *Environ. Sci. DOE/SC-ARM-12−020.*
(40) Lewis, E.; Schwartz, S. *Sea Salt Aerosol Production: Mechanisms, Methods, Measurements, and Models*; Washington, DC, 2004.
(41) de Leeuw, G.; Andreas, E. L.; Anguelova, M. D.; Fairall, C. W.; Lewis, E. R.; O'Dowd, C.; Schulz, M.; Schwartz, S. E. Production Flux of Sea Spray Aerosol. *Rev. Geophys.* **2011**, *49* (2), RG2001.
(42) Gong, S. L. A Parameterization of Sea-Salt Aerosol Source Function for Sub- and Super-Micron Particles. *Global Biogeochem. Cycles* **2003**, *17* (4), 1−7.
(43) Cziczo, D. J.; Thomson, D. S.; Thompson, T. L.; DeMott, P. J.; Murphy, D. M. Particle Analysis by Laser Mass Spectrometry (PALMS) Studies of Ice Nuclei and Other Low Number Density Particles. *Int. J. Mass Spectrom.* **2006**, *258* (1−3), 21−29.
(44) Murphy, D. M. The Design of Single Particle Laser Mass Spectrometers. *Mass Spectrom. Rev.* **2007**, *26* (2), 150−165.
(45) Murphy, D. M.; Thomson, D. S.; Middlebrook, A. M.; Schein, M. E. In Situ Single-Particle Characterization at Cape Grim. *J. Geophys. Res. Atmos.* **1998**, *103* (D13), 16485−16491.
(46) Garimella, S.; Kristensen, T. B.; Ignatius, K.; Welti, A.; Voigtländer, J.; Kulkarni, G. R.; Sagan, F.; Kok, G. L.; Dorsey, J.; Nichman, L.; Rothenberg, D. A.; Rösch, M.; Kirchgäßner, A. C. R.; Ladkin, R.; Wex, H.; Wilson, T. W.; Ladino, L. A.; Abbatt, J. P. D.; Stetzer, O.; Lohmann, U.; Stratmann, F.; Cziczo, D. J. The SPectrometer for Ice Nuclei (SPIN): An Instrument to Investigate Ice Nucleation. *Atmos. Meas. Tech.* **2016**, *9* (7), 2781−2795.
(47) Kulkarni, G.; Kok, G. Mobile Ice Nucleus Spectrometer. *Pacific Northwest Natl. Lab. Richland, WA* 2012.
(48) DeMott, P. J.; Prenni, A. J.; McMeeking, G. R.; Sullivan, R. C.; Petters, M. D.; Tobo, Y.; Niemand, M.; Möhler, O.; Snider, J. R.; Wang, Z.; Kreidenweis, S. M. Integrating Laboratory and Field Data to Quantify the Immersion Freezing Ice Nucleation Activity of Mineral Dust Particles. *Atmos. Chem. Phys.* **2015**, *15* (1), 393−409.
(49) Garimella, S.; Rothenberg, D. A.; Wolf, M. J.; David, R. O.; Kanji, Z. A.; Wang, C.; Rösch, M.; Cziczo, D. J. Uncertainty in Counting Ice Nucleating Particles with Continuous Flow Diffusion Chambers. *Atmos. Chem. Phys.* **2017**, *17* (17), 10855−10864.
(50) Yoon, Y. J.; Ceburnis, D.; Cavalli, F.; Jourdan, O.; Putaud, J. P.; Facchini, M. C.; Decesari, S.; Fuzzi, S.; Sellegri, K.; Jennings, S. G.; O'dowd, C. D. Seasonal Characteristics of the Physicochemical Properties of North Atlantic Marine Atmospheric Aerosols. *J. Geophys. Res.* **2007**, *112* DOI: 10.1029/2005JD007044.
(51) Facchini, M. C.; Rinaldi, M.; Decesari, S.; Carbone, C.; Finessi, E.; Mircea, M.; Fuzzi, S.; Ceburnis, D.; Flanagan, R.; Nilsson, E. D.; de Leeuw, G.; Martino, M.; Woeltjen, J.; O'Dowd, C. D. Primary Submicron Marine Aerosol Dominated by Insoluble Organic Colloids and Aggregates. *Geophys. Res. Lett.* **2008**, *35* (17), L17814.
(52) Prather, K. A.; Bertram, T. H.; Grassian, V. H.; Deane, G. B.; Stokes, M. D.; Demott, P. J.; Aluwihare, L. I.; Palenik, B. P.; Azam, F.; Seinfeld, J. H.; Moffet, R. C.; Molina, M. J.; Cappa, C. D.; Geiger, F. M.; Roberts, G. C.; Russell, L. M.; Ault, A. P.; Baltrusaitis, J.; Collins, D. B.; Corrigan, C. E.; Cuadra-Rodriguez, L. A.; Ebben, C. J.; Forestieri, S. D.; Guasco, T. L.; Hersey, S. P.; Kim, M. J.; Lambert, W. F.; Modini, R. L.; Mui, W.; Pedler, B. E.; Ruppel, M. J.; Ryder, O. S.; Schoepp, N. G.; Sullivan, R. C.; Zhao, D. Bringing the Ocean into the Laboratory to Probe the Chemical Complexity of Sea Spray Aerosol. *Proc. Natl. Acad. Sci. U. S. A.* **2013**, *110* (19), 7550−7555.
(53) Wang, X.; Deane, G. B.; Moore, K. A.; Ryder, O. S.; Stokes, M. D.; Beall, C. M.; Collins, D. B.; Santander, M. V.; Burrows, S. M.; Sultana, C. M.; Prather, K. A. The Role of Jet and Film Drops in Controlling the Mixing State of Submicron Sea Spray Aerosol Particles. *Proc. Natl. Acad. Sci. U. S. A.* **2017**, *114* (27), 6978−6983.
(54) Wise, M. E.; Martin, S. T.; Russell, L. M.; Buseck, P. R. Water Uptake by NaCl Particles Prior to Deliquescence and the Phase Rule. *Aerosol Sci. Technol.* **2008**, *42* (4), 281−294.
(55) Khvorostyanov, V. I.; Curry, J. A. The Theory of Ice Nucleation by Heterogeneous Freezing of Deliquescent Mixed CCN. Part I: Critical Radius, Energy, and Nucleation Rate. *J. Atmos. Sci.* **2004**, *61* (22), 2676−2691.
(56) Graether, S. P.; Jia, Z. Modeling Pseudomonas Syringae Ice-Nucleation Protein as a Beta-Helical Protein. *Biophys. J.* **2001**, *80* (3), 1169−1173.
(57) Budke, C.; Dreyer, A.; Jaeger, J.; Gimpel, K.; Berkemeier, T.; Bonin, A. S.; Nagel, L.; Plattner, C.; DeVries, A. L.; Sewald, N.; Koop, T. Quantitative Efficacy Classification of Ice Recrystallization Inhibition Agents. *Cryst. Growth Des.* **2014**, *14* (9), 4285−4294.
(58) Gonda, T.; Sei, T. The Inhibitory Growth Mechanism of Saccharides on the Growth of Ice Crystals from Aqueous Solutions. *Prog. Cryst. Growth Charact. Mater.* **2005**, *51* (1−3), 70−80.
(59) Peng, C.; Chow, A. H. L.; Chan, C. K. Hygroscopic Study of Glucose, Citric Acid, and Sorbitol Using an Electrodynamic Balance: Comparison with UNIFAC Predictions. *Aerosol Sci. Technol.* **2001**, *35*, 753−758.
(60) Chan, M. N.; Kreidenweis, S. M.; Chan, C. K. Measurements of the Hygroscopic and Deliquescence Properties of Organic Compounds of Different Solubilities in Water and Their Relationship with Cloud Condensation Nuclei Activities. *Environ. Sci. Technol.* **2008**, *42* (10), 3602−3608.
(61) Murray, B. J.; Wilson, T. W.; Dobbie, S.; Cui, Z.; Al-Jumur, S. M. R. K.; Möhler, O.; Schnaiter, M.; Wagner, R.; Benz, S.; Niemand, M.; Saathoff, H.; Ebert, V.; Wagner, S.; Kärcher, B. Heterogeneous Nucleation of Ice Particles on Glassy Aerosols under Cirrus Conditions. *Nat. Geosci.* **2010**, *3* (4), 233−237.
(62) Ignatius, K.; Kristensen, T. B.; Järvinen, E.; Nichman, L.; Fuchs, C.; Gordon, H.; Herenz, P.; Hoyle, C. R.; Duplissy, J.; Garimella, S.; Dias, A.; Frege, C.; Höppel, N.; Tröstl, J.; Wagner, R.; Yan, C.; Amorim, A.; Baltensperger, U.; Curtius, J.; Donahue, N. M.; Gallagher, M. W.; Kirkby, J.; Kulmala, M.; Möhler, O.; Saathoff, H.; Schnaiter, M.; Tomé, A.; Virtanen, A.; Worsnop, D.; Stratmann, F. Heterogeneous Ice Nucleation of Viscous Secondary Organic Aerosol Produced from Ozonolysis of a-Pinene. *Atmos. Chem. Phys.* **2016**, *16* (10), 6495−6509.
(63) Berkemeier, T.; Shiraiwa, M.; Pöschl, U.; Koop, T. Competition between Water Uptake and Ice Nucleation by Glassy Organic Aerosol Particles. *Atmos. Chem. Phys.* **2014**, *14*, 12513−12531.
(64) Koop, T.; Bookhold, J.; Angell, C. A.; Mikkila, J.; et al. Glass Transition and Phase State of Organic Compounds: Dependency on

DOI: 10.1021/acs.est.8b05150
Environ. Sci. Technol. 2019, 53, 1139−1149

Molecular Properties and Implications for Secondary Organic Aerosols in the Atmosphere. *Phys. Chem. Chem. Phys.* **2011**, *13* (43), 19238.
(65) DeRieux, W.-S. W.; Li, Y.; Lin, P.; Laskin, J.; Laskin, A.; Bertram, A. K.; Nizkorodov, S. A.; Shiraiwa, M. Predicting the Glass Transition Temperature and Viscosity of Secondary Organic Material Using Molecular Composition. *Atmos. Chem. Phys.* **2018**, *18* (9), 6331−6351.
(66) Green, M. M.; Blankenhorn, G.; Hart, H. Which Starch Fraction Is Water Soluble, Amylose or Amylopectin? *J. Chem. Educ.* **1975**, *52* (11), 729−730.
(67) Pummer, B. G.; Budke, C.; Augustin-Bauditz, S.; Niedermeier, D.; Felgitsch, L.; Kampf, C. J.; Huber, R. G.; Liedl, K. R.; Loerting, T.; Moschen, T.; Schauperl, M.; Tollinger, M.; Morris, C. E.; Wex, H.; Grothe, H.; Pöschl, U.; Koop, T.; Fröhlich-Nowoisky, J. Ice Nucleation by Water-Soluble Macromolecules. *Atmos. Chem. Phys.* **2015**, *15* (8), 4077−4091.
(68) Pummer, B. G.; Bauer, H.; Bernardi, J.; Bleicher, S.; Grothe, H. Suspendable Macromolecules Are Responsible for Ice Nucleation Activity of Birch and Conifer Pollen. *Atmos. Chem. Phys.* **2012**, *12* (5), 2541−2550.
(69) Ullrich, R.; Hoose, C.; Möhler, O.; Niemand, M.; Wagner, R.; Höhler, K.; Hiranuma, N.; Saathoff, H.; Leisner, T. A New Ice Nucleation Active Site Parameterization for Desert Dust and Soot. *J. Atmos. Sci.* **2017**, *74* (3), 699−717.
(70) Welti, A.; Lüönd, F.; Stetzer, O.; Lohmann, U. Influence of Particle Size on the Ice Nucleating Ability of Mineral Dusts. *Atmos. Chem. Phys.* **2009**, *9* (18), 6705−6715.
(71) Hiranuma, N.; Hoffmann, N.; Kiselev, A.; Dreyer, A.; Zhang, K.; Kulkarni, G.; Koop, T.; Möhler, O. Influence of Surface Morphology on the Immersion Mode Ice Nucleation Efficiency of Hematite Particles. *Atmos. Chem. Phys.* **2014**, *14* (5), 2315−2324.
(72) Steinke, I.; Hoose, C.; Möhler, O.; Connolly, P.; Leisner, T. A New Temperature- and Humidity-Dependent Surface Site Density Approach for Deposition Ice Nucleation. *Atmos. Chem. Phys.* **2015**, *15* (7), 3703−3717.
(73) Steinke, I.; Funk, R.; Busse, J.; Iturri, A.; Kirchen, S.; Leue, M.; Möhler, O.; Schwartz, T.; Schnaiter, M.; Sierau, B.; Toprak, E.; Ullrich, R.; Ulrich, A.; Hoose, C.; Leisner, T. Ice Nucleation Activity of Agricultural Soil Dust Aerosols from Mongolia, Argentina, and Germany. *J. Geophys. Res. Atmos.* **2016**, *121* (22), 13559−13576.
(74) Cochran, R. E.; Laskina, O.; Trueblood, J. V.; Estillore, A. D.; Morris, H. S.; Jayarathne, T.; Sultana, C. M.; Lee, C.; Lin, P.; Laskin, J.; Laskin, A.; Dowling, J. A.; Qin, Z.; Cappa, C. D.; Bertram, T. H.; Tivanski, A. V.; Stone, E. A.; Prather, K. A.; Grassian, V. H. Molecular Diversity of Sea Spray Aerosol Particles: Impact of Ocean Biology on Particle Composition and Hygroscopicity. *Chem.* **2017**, *2* (5), 655−667.
(75) Bursa, A. S. Starch in the Oceans. *J. Fish. Res. Board Can.* **1968**, *25* (6), 1269−1284.
(76) Pernthaler, J. Predation on Prokaryotes in the Water Column and Its Ecological Implications. *Nat. Rev. Microbiol.* **2005**, *3* (7), 537−546.
(77) O'Dowd, C. D.; Langmann, B.; Varghese, S.; Scannell, C.; Ceburnis, D.; Facchini, M. C. A Combined Organic-Inorganic Sea-Spray Source Function. *Geophys. Res. Lett.* **2008**, *35* (1), L01801.
(78) Burrows, S. M.; Hoose, C.; Pöschl, U.; Lawrence, M. G. Ice Nuclei in Marine Air: Biogenic Particles or Dust? *Atmos. Chem. Phys.* **2013**, *13* (1), 245−267.
(79) Vergara-Temprado, J.; Murray, B. J.; Wilson, T. W.; O'Sullivan, D.; Browse, J.; Pringle, K. J.; Ardon-Dryer, K.; Bertram, A. K.; Burrows, S. M.; Ceburnis, D.; DeMott, P. J.; Mason, R. H.; O'Dowd, C. D.; Rinaldi, M.; Carslaw, K. S. Contribution of Feldspar and Marine Organic Aerosols to Global Ice Nucleating Particle Concentrations. *Atmos. Chem. Phys.* **2017**, *17* (5), 3637−3658.
(80) Sarmiento, J. L.; Gruber, N. *Ocean Biogeochemical Dynamics*; Princeton University Press, 2006.
(81) Graham, A.; Woolf, D. K.; Hall, A. J.; Graham, A.; Woolf, D. K.; Hall, A. J. Aeration Due to Breaking Waves. Part I: Bubble Populations. *J. Phys. Oceanogr.* **2004**, *34* (5), 989−1007.
(82) Koop, T.; Luo, B.; Tsias, A.; Peter, T. Water Activity as the Determinant for Homogeneous Ice Nucleation in Aqueous Solutions. *Nature* **2000**, *406* (6796), 611−614.

DOI: 10.1021/acs.est.8b05150
Environ. Sci. Technol. 2019, 53, 1139−1149